

Stubborn: A Streamlined and Unified Reinforcement Learning Framework for Robust Motion Tracking and Fall Recovery for Humanoids

Xiao Ren*, Yuhui Yang*, Zongbiao Weng, Zhijie Liu, and He Kong[†]

Abstract: Recent reinforcement learning approaches have shown great promise in improving humanoid motion tracking performance and achieving fall recovery under disturbances. However, most existing works treat motion tracking and fall recovery as different tasks and require multi-stage training with specialized recovery rewards and/or separate recovery policies. Moreover, existing reinforcement learning-based methods often terminate training episodes immediately after severe tracking failures, limiting recovery-oriented exploration in unstable or fallen states. To address the above issues, we propose Stubborn, a streamlined and unified reinforcement learning framework to achieve robust humanoid motion tracking and fall recovery. Specifically, Stubborn uses an asymmetric Actor-Critic architecture and consists of three major components. First, a yaw-aligned tracking representation is adopted to reduce sensitivity to global drift and heading disturbances while preserving gravity-related balance information. Second, we introduce a Bernoulli-based probabilistic termination mechanism that enables the policy to encourage exploration of fall-recovery behaviors under varying failure modes. Third, we propose a probabilistic termination and tracking-error-driven strategy that dynamically reshapes the sampling distribution based on tracking performance, increasing the training efficiency for difficult motion segments and unstable states. Extensive comparisons with SOTA methods and ablation studies show that Stubborn achieved competitive performance, and the proposed probabilistic termination mechanism and adaptive sampling strategy contributed to the performance and robustness gains. For real-world demonstrations, please refer to <https://aislab-sustech.github.io/Stubborn/>.

Keywords: Humanoids, reinforcement learning, motion tracking, fall recovery

1 Introduction

Recent years have witnessed much progress in reinforcement learning-based highly dynamic motion tracking for humanoids, including dancing [1, 2, 3] and martial arts [4, 5]. There exist works that rely on global absolute pose tracking for training, which might cause the policy to exert excessive control effort to correct translation and heading deviations after perturbations [6, 7]. To address the above issue, recent works in the literature adopt a yaw-aligned tracking representation to reduce sensitivity to global drift and heading disturbances while preserving gravity-related balance information [8, 9].

Although existing reinforcement learning (RL) methods can achieve remarkable performance under normal conditions, maintaining tracking accuracy and robustness (e.g., recovering from falls) under strong external disturbances remains a challenging problem [10, 11, 12]. In particular, how to enhance tracking performance and robustness in an effective and unified way, rather than treating

*Xiao Ren and Yuhui Yang contributed equally to this work. The authors are with the Southern University of Science and Technology, Shenzhen 518055, China. E-mails: [12431359;12411024;12433032;12332642]@mail.sustech.edu.cn, kongh@sustech.edu.cn.

[†]Corresponding author.

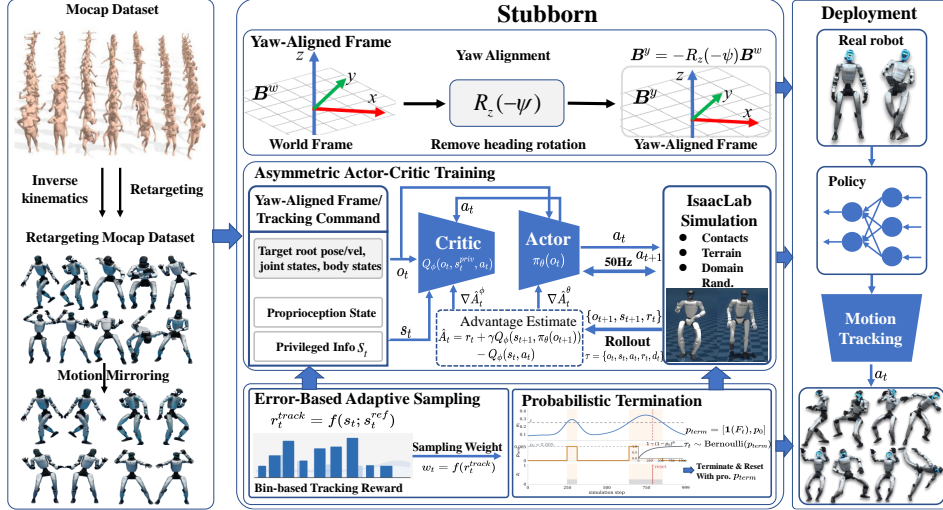


Figure 1: **Overview of Stubborn.** The policy is trained with a yaw-aligned representation and via an asymmetric actor-critic architecture, with a Bernoulli-based soft termination mechanism, and probabilistic termination and tracking error-driven sampling strategy.

motion tracking and fall recovery as separate tasks, has not been well explored and several design issues remain to be addressed.

In particular, under long-horizon training, uniformly sampled training data often under-represent difficult motion segments and unstable states, limiting the exploration capability of the policy [13, 14]. In addition, for fall recovery, most existing methods employ hard termination mechanisms: once the tracking error exceeds a predefined threshold, the policy training terminates (or, during deployment, the execution terminates). Such designs would prematurely prevent the policy from exploring to learn to recover. Existing studies often address this issue through recovery-specific rewards, multi-stage training procedures, or separate recovery controllers [15, 16], thus increasing the architectural or training complexity.

To address these challenges, we propose Stubborn, a streamlined and unified RL framework for training a single policy to achieve robust humanoid motion tracking and fall recovery. As shown in Figure 1, Stubborn uses a unified single policy for tracking highly dynamic motions while maintaining robustness under strong perturbations and achieving recovery from fallen states. Stubborn adopts an asymmetric Actor-Critic architecture [17] with yaw-aligned tracking representation, where the value network uses privileged simulation information, while the policy network relies only on proprioceptive observations. On this basis, we make the following contributions: (1) We propose a Bernoulli-based soft termination mechanism that encourages the policy to learn resilient actions in unstable and fallen states, thereby synthesizing emergent recovery behaviors without auxiliary recovery-specific reward design. (2) We develop a probabilistic termination (PT) and tracking error-driven sampling strategy that dynamically reshapes the sampling distribution based on on-line tracking performance, thereby improving learning efficiency in difficult tracking and recovery states. (3) Extensive simulations and real-world experiments on the 29-DoF Unitree G1 humanoid robot demonstrate that Stubborn achieves competitive performance against SOTA methods [18, 19, 20, 13]. Ablation studies have also shown that the proposed probabilistic termination mechanism and adaptive sampling strategy contribute to performance gains.

2 Related Work

Humanoid Motion Tracking: In recent years, reinforcement learning has become a common paradigm for humanoid motion imitation and tracking [6, 13, 21, 22]. For example, DeepMimic [6]

learns physics-based controllers by tracking reference motion clips with imitation objectives. BeyondMimic [13] learns motion-tracking primitives for highly dynamic humanoid skills through adaptive sampling and distills the learned primitives into a guided diffusion policy for downstream humanoid control. HumanPlus [21] and OmniH2O [22] primarily target whole-body imitation, teleoperation, and autonomous behavior learning, rather than unified motion tracking in highly dynamic, long-horizon settings. ASAP [23] improves sim-to-real transfer for agile humanoid skills through real-to-sim-to-real adaptation, while GMT [14] improves general motion tracking through large-scale motion data, adaptive sampling, and a motion mixture-of-experts architecture. HoloMotion [18] explores foundation models for whole-body control to improve diverse motion generation and tracking, while BFM-Zero [20] focuses on zero-shot and few-shot robot motion transfer.

Motion tracking is closely related to whole-body control [24], and data-driven whole-body control methods have further advanced this direction. ExBody2 [25, 26] emphasizes stable whole-body imitation under diverse reference motions. TWIST [27, 28] and CLONE [29] improve long-horizon whole-body control through real-time teleoperation and closed-loop correction, respectively. SONIC [30] further explores scaling motion tracking toward general whole-body behaviors. Although recent work continues to advance unified data-driven representations and broader generalization, challenges remain in robustness under strong perturbations, learning difficult long-horizon motion segments, and handling tracking and recovery within a unified framework.

Robustness and Fall Recovery: Motion robustness and autonomous fall recovery are important capabilities for humanoid robots in practice. RL-based methods have been widely used to train standing-up and push-recovery policies for humanoids [31, 32, 33]. For example, HoST [34] improves recovery across diverse poses through a multi-critic architecture and curriculum learning, while HumanUP [35] learns standing-up policies across multiple terrains and initial fall states. HuB [36] improves humanoid balance robustness by combining reference motion refinement, balance-aware policy learning, and robustness training. Although the above-mentioned methods help to learn recovery and balance behaviors, policies are typically designed for specific recovery or balance scenarios, separately from the motion tracking policy, requiring extensive reward tuning. Unlike recovery-specific policy learning, recent studies have also improved robustness from the perspective of motion tracking. For example, Any2Track [19] adopts a two-stage tracker-adapter framework to improve motion tracking robustness under disturbances and sim-to-real variations.

Overall, existing works often treat motion tracking and fall recovery as competing objectives with conflicting gradients [31]. To decouple these tasks, the community seeks solutions using multi-stage training and separate recovery policies with recovery-specific rewards. We argue that tracking failures actually provide a natural gateway to the fall state manifold. By harnessing these natural transitions rather than avoiding them, one might achieve high-fidelity motion tracking, robustness to strong perturbations, and recovery from unstable states with a unified training framework and policy. This is the objective that this paper aims to fulfill. Our framework spontaneously explores recovery behaviors alongside motion tracking, enabling highly sample-efficient, simultaneous exploration of both tasks within a single policy.

3 Method

Stubborn, as illustrated in Figure 1, is trained using an asymmetric actor-critic architecture and consists of three core modules. Due to limited space, details of the drift-invariant yaw-aligned tracking representation are placed in the Appendix section while the Bernoulli-based PT mechanism, as well as the PT and tracking error-driven sampling strategy are described in the following.

3.1 Bernoulli-based Probabilistic Termination for Fall Recovery Learning

Conditional Bernoulli Termination Mechanism: In our framework, when the tracking error exceeds a predefined threshold, the environment does not terminate the episode deterministically; instead, it triggers a termination with a user-specified probability. More specifically, we denote the height error $e_{root,z}^p$ of the robot’s floating base and the orientation error e_{root}^a , computed via the

quaternion inner product in SO(3), as follows:

$$e_{root,z}^p = p_{root,z}^{ref} - p_{root,z}, \quad e_{root}^q = 2 \arccos \left(\left| \langle q_{root}^{ref}, q_{root} \rangle \right| \right). \quad (1)$$

Let $\tau_t \in \{0, 1\}$ denote the binary termination indicator at time step t . We model this indicator via a conditional Bernoulli distribution:

$$P(\tau_t = 1 \mid s_t) = \begin{cases} p_{term}, & (|e_{root,z}^p| > \theta_{pos}) \vee (e_{root}^q > \theta_{quat}) \\ 0, & \text{otherwise} \end{cases}, \quad (2)$$

where s_t represents the system state. The termination probability p_{term} is designed to accommodate the physical time window required for fall recovery, thereby mitigating value estimation bias caused by standard time-limit truncation. In the following, we provide guidelines for selecting p_{term} .

Design of the Termination Probability: If the robot remains in a marginally stable state after exceeding the tracking error threshold, the number of additional survival steps before episode termination can be modeled as a random variable $\mathcal{T} \sim Geo(p_{term})$. To maintain consistent temporal difference (TD) updates, the expectation of \mathcal{T} should align with the physical recovery time:

$$\mathbb{E}[\mathcal{T}] = \frac{1}{p_{term}} = f_{ctrl} \cdot t_{rec}, \quad (3)$$

where $f_{ctrl} = 50$ Hz is the control frequency. We set the physical recovery time to $t_{rec} = 4$ s, which provides the policy with an expected exploration horizon of 200 steps ($\mathbb{E}[\mathcal{T}] = 200$). A window that is too restrictive can degenerate the mechanism into a deterministic one, thus hindering the learning of recovery behaviors, and vice versa. Following this design guideline, we select $p_{term} = 0.005$, and set the thresholds to $\theta_{pos} = 0.25$ m and $\theta_{quat} = \frac{\pi}{2}$ rad in our experiments.

Under this mechanism, after the tracking error exceeds the threshold, the episode continues at each subsequent step with probability $1 - p_{term}$. Let k denote the number of additional control steps after entering the unstable region; then the probability that the episode remains active for more than k steps is $P(\mathcal{T} > k) = (1 - p_{term})^k$. This design reduces immediate termination after disturbances or falls and provides a probabilistic recovery window for learning recovery behaviors toward post-perturbation stable tracking. Furthermore, assuming a perturbation occurs early in the episode, under an ideal exploration window with a maximum episode length ($T_{max} = 1000$), the cumulative probability of terminating prior to the step limit is given by $P(\mathcal{T} \leq T_{max}) = 1 - (1 - p_{term})^{T_{max}}$. Substituting our selected parameters ($p_{term} = 0.005$, $T_{max} = 1000$), this probability evaluates to approximately 0.993. The parameter p_{term} , derived from physical recovery constraints, ensures that the vast majority ($> 99\%$) of unstable episodes terminate probabilistically before reaching the step limit. This substantially mitigates the TD distortion caused by truncation and promotes the stability of long-horizon optimization.

3.2 Probabilistic Termination and Tracking Error Driven Sampling

Under hard termination, segments with tracking errors exceeding a predefined threshold are more likely to terminate the episode early [13]. However, under the PT mechanism described in Section 3.1, segments exceeding the error threshold are not terminated immediately; instead, the episode terminates only with a certain probability. As a result, episode termination is no longer a reliable proxy for segment difficulty, since it is affected by stochastic termination and external perturbations. Consequently, the correspondence between termination statistics and segment difficulty is weakened, making hard-sample mining based on termination statistics less reliable. To address this issue, we propose a probabilistic termination and tracking-error-driven adaptive sampling strategy.

Let the total length of the reference trajectory be N , and let w_t denote the unnormalized sampling weight associated with reference frame t . At each environment reset, an initial frame t_0 is sampled according to the normalized sampling distribution, and an episode of maximum length T_{max} is executed from that frame. Let T denote the actual episode length, where $1 \leq T \leq T_{max}$, and let $e_{kp,t}$ denote the instantaneous keypoint tracking error at reference frame t . Then, for an episode

starting at t_0 and lasting T steps, the average keypoint tracking error is defined as

$$\bar{e} = \frac{1}{T} \sum_{k=0}^{T-1} e_{\text{kp}, t_0+k}, \quad (4)$$

where \bar{e} represents the average keypoint tracking error over the current reference segment. For each time step $t \in [t_0, t_0 + T - 1]$ within the sampled segment, the weight increment Δw_t is defined as

$$\Delta w_t = \begin{cases} +\Delta w_i, & \bar{e} \geq \theta_{\text{success}}, \\ \Phi_{\text{att}}(t), & \bar{e} < \theta_{\text{success}} \wedge T = T_{\text{max}}, \\ \Phi_{\text{dist}}(t), & \bar{e} < \theta_{\text{success}} \wedge T < T_{\text{max}}. \end{cases} \quad (5)$$

Here, θ_{success} denotes the success threshold for the average tracking error, and we set $\theta_{\text{success}} = 0.06$ in our implementation. A segment is regarded as successfully tracked when $\bar{e} < \theta_{\text{success}}$; otherwise, it is considered to require further training. Moreover, $\Delta w_i > 0$ and $\Delta w_d > 0$ denote the step sizes for increasing and decreasing the sampling weights, respectively. In our implementation, $\Delta w_i = 0.10$ and $\Delta w_d = 0.05$. When an episode reaches the maximum length T_{max} while maintaining a low average error, the local decay operator $\Phi_{\text{att}}(t)$ is applied. When an episode satisfies $\bar{e} < \theta_{\text{success}}$ but terminates before reaching the maximum length, i.e., $T < T_{\text{max}}$, the local redistribution operator $\Phi_{\text{dist}}(t)$ is applied. They are defined as

$$\Phi_{\text{att}}(t) = \begin{cases} -2\Delta w_d, & t < t_0 + \lfloor T/2 \rfloor, \\ -\Delta w_d, & \text{otherwise,} \end{cases}, \quad \Phi_{\text{dist}}(t) = \begin{cases} -2\Delta w_d, & t < t_0 + \lfloor T/3 \rfloor, \\ -\Delta w_d, & t < t_0 + \lfloor T/2 \rfloor, \\ 0, & t < t_0 + \lfloor 2T/3 \rfloor, \\ +\Delta w_i, & \text{otherwise.} \end{cases} \quad (6)$$

Subsequently, the sampling weights of the reference frames involved in the current episode are updated as follows: where w_{min} and w_{max} denote the lower and upper bounds of the sampling weights, respectively. In our implementation, we set $w_{\text{min}} = 0.05$ and $w_{\text{max}} = 1.0$. After the update, the weights are normalized to obtain the sampling distribution for selecting the starting frame of the next episode as follows $p_t = \frac{\max(w_t, w_{\text{min}})}{\sum_{j=0}^{N-1} \max(w_j, w_{\text{min}})}$. In this way, the online tracking error \bar{e} serves as an empirical indicator of segment difficulty, allowing the sampling distribution to adapt dynamically even under the probabilistic termination mechanism. As a result, more probability mass is assigned to high-error regions, encouraging training to focus on difficult motion segments. The overall algorithm of Stubborn is summarized in Algorithm 1 in Appendix.

4 Results and Discussions

This section provides a systematic evaluation of Stubborn through both simulation and real experiments, with a focus on the following four questions: **Q1**: How does Stubborn compare with baseline methods on large and diverse motion datasets, and how well does it generalize to unseen motions? **Q2**: Does the PT mechanism improve disturbance recovery and fall recovery capability under strong perturbations? **Q3**: Does the proposed PT and tracking error-driven sampling strategy improve tracking performance across diverse motion skills? **Q4**: How does Stubborn perform in real-world scenarios?

4.1 Experiment Setup

Simulation experiments are conducted in IsaacLab/MuJoCo using motions from the public LAFAN1 [37] dataset. Real-robot experiments are performed on the 29-DoF Unitree G1 humanoid robot with retargeted motions from LAFAN1 [37] and AMASS [38] to evaluate the practical deployability of the learned policy.

Baselines. We compare Stubborn with representative humanoid motion tracking methods, including HoloMotion [18], Any2Track [19], BFM-Zero [20], and a From-scratch multi-motion RL baseline [39]. The latter follows BeyondMimic [13] in its algorithmic framework and network architecture, while extending single-motion tracking to end-to-end multi-motion RL training. We do not

directly compare with OmniXtreme [39], as it uses substantially larger-scale motion data and targets general highly dynamic humanoid control, whereas our evaluation focuses on precise motion tracking, robustness, and fall recovery.

Evaluation Metrics and Training Details. For motion tracking, we use root-relative mean per-body position error (MPBPE, mm), mean per-joint position error (MPJPE, 10^{-3} rad), mean per-joint velocity error (MPJVE, 10^{-3} rad/s), and acceleration deviation (Δacc , rad/s^2). For recovery, the robot is subjected to strong external perturbations that may cause unstable tracking, severe balance loss, or complete falls. A trial is successful if the robot re-establishes stable tracking within the predefined tracking-error threshold after the disturbance or fall, and unsuccessful otherwise. The main evaluation metric is the success rate (Succ, %). The reward items and key training configurations are summarized in the Appendix (see Tables 4 and 5, respectively).

4.2 Results on Motion Tracking

To address **Q1**, this section compares the motion tracking accuracy of Stubborn with baseline methods on the full LAFAN1 dataset. All methods were evaluated on the MuJoCo simulation platform, and the results are shown in Table 1, where the results are reported as the mean \pm one standard deviation. Stubborn achieves lower errors in MPBPE, MPJPE, and MPJVE. Compared with From-scratch RL, MPBPE decreases from 62.68 to 48.85, MPJPE decreases from 115.43 to 113.38, and MPJVE decreases from 887.87 to 624.03. These results indicate that the proposed method improves whole-body position tracking and joint velocity tracking performance under the current test settings. Furthermore, the relatively small standard deviations of MPBPE and MPJVE suggest that the evaluation results on the full LAFAN1 dataset are relatively stable.

Table 1: Quantitative results of motion tracking on the complete LAFAN1 dataset. Results are reported as mean \pm standard deviation. Bold indicates the best result.

Method Metric	MPBPE \downarrow	MPJPE \downarrow	MPJVE \downarrow	Δacc \downarrow
HoloMotion [18]	162.92 \pm 0.000	150.65 \pm 0.000	758.56 \pm 0.000	19.47 \pm 0.000
Any2Track [19]	401.26 \pm 0.000	122.44 \pm 0.000	913.41 \pm 0.000	26.44 \pm 0.000
BFM-Zero [20]	214.09 \pm 0.000	299.36 \pm 0.000	1100.88 \pm 0.000	17.07 \pm 0.000
From-scratch RL [13]	62.68 \pm 0.000	115.43 \pm 0.000	887.87 \pm 0.000	27.75 \pm 0.000
Ours	48.85 \pm 0.000	113.38 \pm 0.000	624.03 \pm 0.000	17.09 \pm 0.000

For Δacc , Stubborn achieves a score of 17.09, which is lower than HoloMotion, Any2Track, and From-scratch RL, and is close to BFM-Zero. Although BFM-Zero achieves a slightly lower Δacc value, its MPBPE, MPJPE, and MPJVE are substantially higher than those of Stubborn. Considering these metrics together, Stubborn achieves lower tracking errors across the full LAFAN1 dataset while maintaining stable, smoother dynamic motion performance.

4.3 Ablation Studies

To address **Q2**, we perform an ablation study on the PT mechanism under a strong external perturbation of 5 m/s, as shown in Table 2. We compare the full Stubborn framework with a variant without

Table 2: Ablation study of the probabilistic termination strategy. Bold means better.

Method	Threshold (m)	Success (%) \uparrow
w/o PT	0.15	77.5
	0.25	85.0
Ours	0.15	100
	0.25	100

PT (w/o PT), while keeping all other settings unchanged. We define the recovery threshold as the success criterion based on the tracking error after perturbation. Specifically, recovery is considered successful once the tracking error falls below the threshold again. Here, 0.15 m corresponds to a strict criterion, whereas 0.25 m corresponds to a more moderate one. Under both thresholds, Stubborn with PT achieves a recovery success rate of 100%, while w/o PT achieves 77.5% and 85.0%, respectively. These results indicate that PT improves recovery success under strong perturbations.

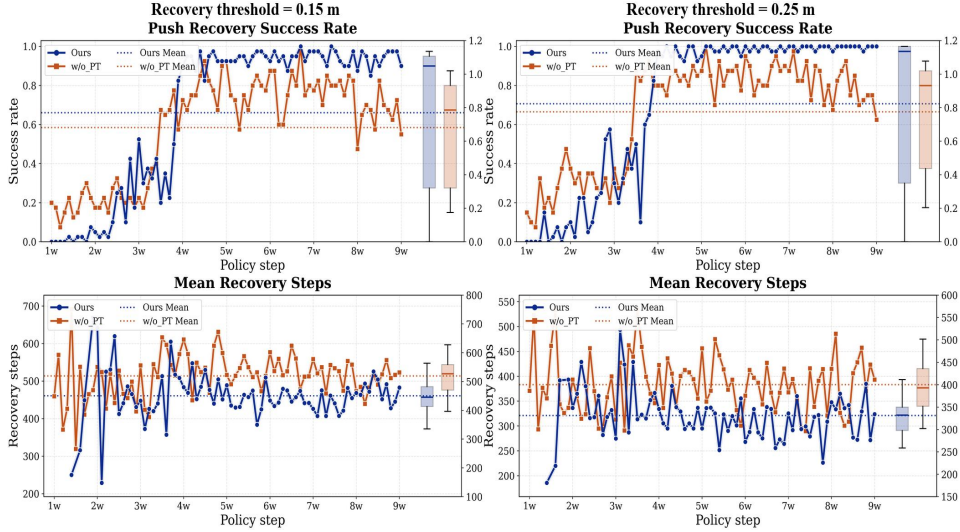


Figure 2: Ablation results of the PT mechanism. The recovery success rate and the average number of recovery steps of Stubborn with PT (Ours) and w/o PT are compared under recovery thresholds of 0.15 m and 0.25 m. Ours achieves higher recovery success rates and requires fewer recovery steps under both recovery thresholds.

Figure 2 shows the recovery success rate and the average number of recovery steps during training under a 5 m/s external perturbation. Ours converges faster and exhibits more stable performance under both thresholds, whereas w/o PT shows larger fluctuations, especially under the stricter threshold of 0.15 m. The box plot on the right summarizes the final-stage evaluation results: the lower and upper whiskers correspond to the 10% and 90% quantiles, respectively, and the solid line inside each box indicates the median. Ours achieves a higher median recovery success rate and requires fewer recovery steps on average than w/o PT, suggesting stronger robustness and more efficient recovery.

Table 3: Ablation study of our proposed sampling strategy. Bold means better.

Method	MPJPE ↓	MPJVE ↓	Δacc ↓
w/o AdpS	120.7	548.5	14.50
Ours	119.4	541.5	14.42

To address Q3, we perform an ablation study on the effect of the adaptive PT and tracking error-driven sampling strategy (AdpS) by comparing the full Stubborn with a variant without this module (w/o AdpS), while keeping all other settings unchanged. As shown in Table 3, introducing AdpS reduces MPJPE, MPJVE, and Δacc from 120.7, 548.5, and 14.50 to 119.4, 541.5, and 14.42, respectively, indicating improved tracking performance in terms of joint position, joint velocity, and acceleration. Figure 3 further illustrates the error trends during training. AdpS maintains lower joint position and velocity errors overall in the middle and late stages, while the acceleration error remains similar to that of w/o AdpS. The box plot on the right summarizes the error distribution in the final training stage, with the solid line within each box indicating the median. These results suggest that tracking-error-based adaptive sampling improves the overall tracking performance of long-horizon, highly dynamic motions by increasing the training frequency for difficult segments.

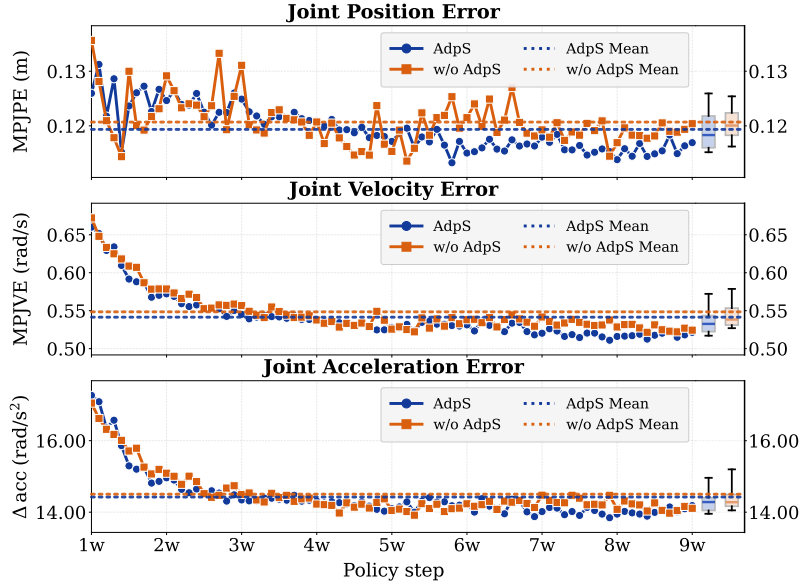


Figure 3: Ablation results of the AdpS sampling strategy. The results suggest that AdpS improves motion-tracking performance in the later training stages.

4.4 Real-World Deployment

To address **Q4**, we evaluate the real-world deployment viability of Stubborn on the physical 29-DoF Unitree G1 humanoid platform, as shown in Figure 4. The real-robot experiments include motions from LAFAN1 [37] and AMASS [38], and demonstrate the robot’s motion tracking, disturbance robustness, and fall recovery performance in physical environments.

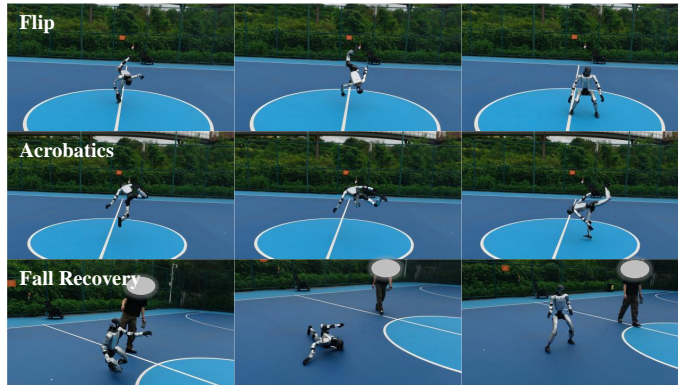


Figure 4: Experimental results. Stubborn can recover from falls and precisely tracks diverse dynamic motions, including flips and acrobatic maneuvers.

5 Conclusion

This paper presents Stubborn, a streamlined and unified RL framework that enables the learning of one policy for robust motion tracking and fall recovery for humanoids. By adopting a yaw-aligned tracking representation, we have proposed a PT mechanism, together with a PT and tracking error-driven sampling strategy. The proposed method improves tracking robustness and enables recovery from both unstable and fallen states under strong perturbations. Experimental results in simulation and on the Unitree G1 humanoid robot demonstrate that Stubborn offers effective disturbance re-

covery, fall recovery, and competitive motion tracking performance under challenging conditions, in comparison with STOA methods. Future work will focus on improving the agility and smoothness of recovery motions after severe falls, as well as extending the framework to more challenging terrains and highly dynamic humanoid behaviors.

References

- [1] X. B. Peng, Z. Ma, P. Abbeel, S. Levine, and A. Kanazawa. Amp: Adversarial motion priors for stylized physics-based character control. *ACM Transactions on Graphics (ToG)*, 40(4): 1–20, 2021.
- [2] Z. Luo, J. Cao, A. Winkler, K. Kitani, and W. Xu. Perpetual humanoid control for real-time simulated avatars. In *Proceedings of the IEEE/CVF International Conference on Computer Vision*, pages 10895–10904, 2023.
- [3] Z. Sun, Y. Peng, Y. Meng, X. Li, B.-S. Huang, Z. Bing, X. Wang, and A. Knoll. Robotdancing: Residual-action reinforcement learning enables robust long-horizon humanoid motion tracking. *arXiv:2509.20717*, 2025.
- [4] W. Xie, J. Han, J. Zheng, H. Li, X. Liu, J. Shi, W. Zhang, C. Bai, and X. Li. Kungfubot: Physics-based humanoid whole-body control for learning highly-dynamic skills. *arXiv:2506.12851*, 2025.
- [5] J. Han, W. Xie, J. Zheng, J. Shi, W. Zhang, T. Xiao, and C. Bai. Kungfubot2: Learning versatile motion skills for humanoid whole-body control. *arXiv:2509.16638*, 2025.
- [6] X. B. Peng, P. Abbeel, S. Levine, and M. Van de Panne. Deepmimic: Example-guided deep reinforcement learning of physics-based character skills. *ACM Transactions On Graphics (TOG)*, 37(4):1–14, 2018.
- [7] T. Zhu, G. Cai, Z. Yang, G. Ren, H. Xie, Z. Wang, J. Wu, J. Wang, X. Yang, Y. Mu, and Y. Yan. Clot: Closed-loop global motion tracking for whole-body humanoid teleoperation. *arXiv:2602.15060*, 2026.
- [8] J. Cheng, D. Kang, G. Fadini, G. Shi, and S. Coros. Rambo: RL-augmented model-based whole-body control for loco-manipulation. *IEEE Robotics and Automation Letters*, 2025.
- [9] H. J. Lee, S. H. Jeon, and S. Kim. Learning humanoid arm motion via centroidal momentum regularized multi-agent reinforcement learning. *IEEE Robotics and Automation Letters*, 2025.
- [10] K. Yin, W. Zeng, K. Fan, M. Dai, Z. Wang, Q. Zhang, Z. Tian, J. Wang, J. Pang, and W. Zhang. Unitracker: Learning universal whole-body motion tracker for humanoid robots. *arXiv:2507.07356*, 2025.
- [11] F. Wu, X. Nal, J. Jang, W. Zhu, Z. Gu, A. Wu, and Y. Zhao. Learn to teach: Sample-efficient privileged learning for humanoid locomotion over real-world uneven terrain. *IEEE Robotics and Automation Letters*, 2025.
- [12] H. Jung, Z. Gu, Y. Zhao, H.-W. Park, and S. Ha. Ppf: Pre-training and preservative fine-tuning of humanoid locomotion via model-assumption-based regularization. *IEEE Robotics and Automation Letters*, 2025.
- [13] Q. Liao, T. E. Truong, X. Huang, Y. Gao, G. Tevet, K. Sreenath, and C. K. Liu. Beyondmimic: From motion tracking to versatile humanoid control via guided diffusion. *arXiv:2508.08241*, 2025.
- [14] Z. Chen, M. Ji, X. Cheng, X. Peng, X. B. Peng, and X. Wang. Gmt: General motion tracking for humanoid whole-body control. *arXiv:2506.14770*, 2025.

- [15] A. Duburcq, F. Schramm, G. Bo eris, N. Bredeche, and Y. Chevaleyre. Reactive stepping for humanoid robots using reinforcement learning: Application to standing push recovery on the exoskeleton atalante. In *2022 IEEE/RSJ international conference on intelligent robots and systems (IROS)*, pages 9302–9309. IEEE, 2022.
- [16] L. Yang, B. Werner, A. B. Ghansah, and A. D. Ames. Bracing for impact: Robust humanoid push recovery and locomotion with reduced order models. In *2025 IEEE-RAS 24th International Conference on Humanoid Robots (Humanoids)*, pages 728–735. IEEE, 2025.
- [17] I. Radosavovic, T. Xiao, B. Zhang, T. Darrell, J. Malik, and K. Sreenath. Real-world humanoid locomotion with reinforcement learning. *Science Robotics*, 9(89):eadi9579, 2024.
- [18] M. Chen, K. Wang, B. Zhang, Y. Ren, Z. Zhu, X. Ma, Q. Huang, Z. Yang, Y. Wang, and Z. Su. Holomotion: A foundation model for whole-body humanoid control, 2026. URL <https://github.com/HorizonRobotics/HoloMotion>.
- [19] Z. Zhang, J. Guo, C. Chen, J. Wang, C. Lin, Y. Lian, H. Xue, Z. Wang, M. Liu, J. Lyu, et al. Track any motions under any disturbances. *arXiv:2509.13833*, 2025.
- [20] Y. Li, Z. Luo, T. Zhang, C. Dai, A. Kanervisto, A. Tirinzoni, H. Weng, K. Kitani, M. Guzek, A. Touati, et al. Bfm-zero: A promptable behavioral foundation model for humanoid control using unsupervised reinforcement learning. *arXiv:2511.04131*, 2025.
- [21] Z. Fu, Q. Zhao, Q. Wu, G. Wetzstein, and C. Finn. Humanplus: Humanoid shadowing and imitation from humans. *arXiv:2406.10454*, 2024.
- [22] T. He, Z. Luo, X. He, W. Xiao, C. Zhang, W. Zhang, K. Kitani, C. Liu, and G. Shi. Omnih2o: Universal and dexterous human-to-humanoid whole-body teleoperation and learning. *arXiv:2406.08858*, 2024.
- [23] T. He, J. Gao, W. Xiao, Y. Zhang, Z. Wang, J. Wang, Z. Luo, G. He, N. Sobanbab, C. Pan, et al. Asap: Aligning simulation and real-world physics for learning agile humanoid whole-body skills. *arXiv:2502.01143*, 2025.
- [24] F. Liu, Z. Gu, Y. Cai, Z. Zhou, H. Jung, J. Jang, S. Zhao, S. Ha, Y. Chen, D. Xu, et al. Opt2skill: Imitating dynamically-feasible whole-body trajectories for versatile humanoid locomanipulation. *IEEE Robotics and Automation Letters*, 2025.
- [25] X. Cheng, Y. Ji, J. Chen, R. Yang, G. Yang, and X. Wang. Expressive whole-body control for humanoid robots. *arXiv:2402.16796*, 2024.
- [26] M. Ji, X. Peng, F. Liu, J. Li, G. Yang, X. Cheng, and X. Wang. Exbody2: Advanced expressive humanoid whole-body control. *arXiv:2412.13196*, 2024.
- [27] Y. Ze, Z. Chen, J. P. Ara ujo, Z.-a. Cao, X. B. Peng, J. Wu, and C. K. Liu. Twist: Teleoperated whole-body imitation system. *arXiv:2505.02833*, 2025.
- [28] Y. Ze, S. Zhao, W. Wang, A. Kanazawa, R. Duan, P. Abbeel, G. Shi, J. Wu, and C. K. Liu. Twist2: Scalable, portable, and holistic humanoid data collection system. *arXiv:2511.02832*, 2025.
- [29] Y. Li, Y. Lin, J. Cui, T. Liu, W. Liang, Y. Zhu, and S. Huang. Clone: Closed-loop whole-body humanoid teleoperation for long-horizon tasks. In *9th Annual Conference on Robot Learning*, 2025.
- [30] Z. Luo, Y. Yuan, T. Wang, C. Li, S. Chen, F. Castaneda, Z.-A. Cao, J. Li, D. Minor, Q. Ben, et al. Sonic: Supersizing motion tracking for natural humanoid whole-body control. *arXiv:2511.07820*, 2025.

- [31] P. Chen, Y. Wang, C. Luo, W. Cai, and M. Zhao. Hifar: Multi-stage curriculum learning for high-dynamics humanoid fall recovery. In *2025 IEEE/RSJ International Conference on Intelligent Robots and Systems (IROS)*, pages 2908–2915. IEEE, 2025.
- [32] C. Gaspard, M. Duclusaud, G. Passault, M. Daniel, and O. Ly. Frasa: An end-to-end reinforcement learning agent for fall recovery and stand up of humanoid robots. In *2025 IEEE International Conference on Robotics and Automation (ICRA)*, pages 15994–16000. IEEE, 2025.
- [33] T. Egle, Y. Yan, D. Lee, and C. Ott. Enhancing model-based step adaptation for push recovery through reinforcement learning of step timing and region. In *2024 IEEE-RAS 23rd International Conference on Humanoid Robots (Humanoids)*, pages 165–172. IEEE, 2024.
- [34] T. Huang, J. Ren, H. Wang, Z. Wang, Q. Ben, M. Wen, X. Chen, J. Li, and J. Pang. Learning humanoid standing-up control across diverse postures. *arXiv:2502.08378*, 2025.
- [35] X. He, R. Dong, Z. Chen, and S. Gupta. Learning getting-up policies for real-world humanoid robots. *arXiv:2502.12152*, 2025.
- [36] T. Zhang, B. Zheng, R. Nai, Y. Hu, Y.-J. Wang, G. Chen, F. Lin, J. Li, C. Hong, K. Sreenath, et al. Hub: Learning extreme humanoid balance. *arXiv:2505.07294*, 2025.
- [37] F. G. Harvey, M. Yurick, D. Nowrouzezahrai, and C. Pal. Robust motion in-betweening. *ACM Transactions on Graphics (TOG)*, 39(4):60–1, 2020.
- [38] N. Mahmood, N. Ghorbani, N. F. Troje, G. Pons-Moll, and M. J. Black. Amass: Archive of motion capture as surface shapes. In *Proceedings of the IEEE/CVF international conference on computer vision*, pages 5442–5451, 2019.
- [39] Y. Wang, S. Zhu, P. Zhi, Y. Li, J. Li, Y.-L. Li, Y. Xiao, X. Wang, B. Jia, and S. Huang. Omnix-treme: Breaking the generality barrier in high-dynamic humanoid control. *arXiv:2602.23843*, 2026.

6 Appendix

6.1 Drift-Invariant Yaw-Aligned Tracking Representation

To decouple global drift from the desired motion style, similar to [8, 9], our framework adopts a yaw-invariant tracking representation based on a yaw-angle-aligned root coordinate system. Let W denote the world frame and B the robot base frame. The global pose of the robot base remains defined in the world frame, where $T_B^W \in SE(3)$ consists of the rotation $R_B^W \in SO(3)$ and the position $p_B^W \in \mathbb{R}^3$. Using the Z-Y-X Euler-angle convention, R_B^W is decomposed into the product of the yaw angle ψ , pitch angle θ , and roll angle ϕ as $R_B^W = R_Z(\psi)R_Y(\theta)R_X(\phi)$. Accordingly, we define the yaw-aligned frame Ψ , whose homogeneous transformation with respect to W is given by $T_\Psi^W = \begin{bmatrix} R_Z(\psi) & p_B^W \\ 0_{1 \times 3} & 1 \end{bmatrix}$. For any rigid body $i \in \mathcal{B}$, with world-frame pose (R_i^W, p_i^W) , its pose in Ψ is obtained via

$$T_i^\Psi = (T_\Psi^W)^{-1}T_i^W = \begin{bmatrix} R_Z^T(\psi)R_i^W & R_Z^T(\psi)(p_i^W - p_B^W) \\ 0_{1 \times 3} & 1 \end{bmatrix}.$$

The corresponding local position \tilde{p}_i and orientation \tilde{R}_i in the aligned frame are then $\tilde{p}_i = R_Z^T(\psi)(p_i^W - p_B^W)$, $\tilde{R}_i = R_Z^T(\psi)R_i^W$. This representation reduces sensitivity to global drift while preserving key physical cues for motion control. The relative displacement term $(p_i^W - p_B^W)$ removes global translation, while the inverse yaw rotation $R_Z^T(\psi)$ removes the global heading component from the body pose representation. Therefore, the resulting tracking errors mainly reflect local whole-body coordination rather than global translation or yaw drift, reducing unnecessary global correction under strong perturbations. The yaw-aligned transformation is applied to the body tracking representation, while the root pose remains defined in the world frame, enabling the policy to reduce sensitivity to global drift while preserving gravity-related pitch and roll information.

6.2 The Overall Algorithm Pipeline and Training Details of Stubborn

Algorithm 1: The Overall Algorithm Pipeline of Stubborn

Input : $\mathcal{T}_{ref} \in SE(3)^{N \times |\mathcal{B}|}$: Reference trajectory
 π_θ, V_ϕ : Policy and Value networks
 $N_{env}, K_{rollout}$: Env count & rollout length
 $\theta_{success}, \theta_{pos}, \theta_{quat}, p_{term}$: Threshold parameters

Output: θ, ϕ : Optimized network parameters

Init $w_t \leftarrow 1.0, \forall t$; Sample states $s^{(e)} \sim p_t \propto w_t$;
for $iter = 1, 2, \dots$ **do**
 for $k = 1$ **to** K **do**
 $a_k^{(e)} \sim \pi_\theta(\cdot | s_k^{(e)}), s_{k+1}^{(e)} \leftarrow \text{EnvStep}(s_k, a_k)$;
 // Drift-Invariant Yaw-Aligned Tracking Representation
 $T_\Psi^W \leftarrow \text{YawAlign}(T_B^W)$;
 $(\tilde{p}_i, \tilde{R}_i)^{(e)} \leftarrow (T_\Psi^W)^{-1} T_i^W, \forall i \in \mathcal{B}$;
 $r_k^{(e)} \leftarrow \text{Reward}(\{\tilde{p}_i, \tilde{R}_i\})$;
 // Bernoulli-based Probabilistic Termination for Fall Recovery Learning
 for $env e \in \{1, \dots, N_{env}\}$ **do**
 $\rho_k \leftarrow \mathbb{I}(|e_{root,z}^p| > \theta_{pos} \vee e_{root}^q > \theta_{quat})$;
 $\tau_k \sim \text{Bernoulli}(\rho_k \cdot p_{term})$;
 if $T \geq T_{max} \vee \tau_k == 1$ **then**
 // Probabilistic Termination and Tracking Error-driven Sampling
 $\bar{e} \leftarrow \text{MeanErr}(t_0^{(e)}, T)$;
 for $t \in [t_0^{(e)}, t_0^{(e)} + T - 1]$ **do**
 if $\bar{e} \geq \theta_{success}$ **then** $\Delta w_t \leftarrow +\Delta w_i$;
 else if $T \geq T_{max}$ **then** $\Delta w_t \leftarrow \Phi_{att}(t)$;
 else $\Delta w_t \leftarrow \Phi_{dist}(t)$;
 $w_t \leftarrow \max(\min(w_t + \Delta w_t, w_{max}), w_{min})$;
 $p_t \leftarrow w_t / \sum w_j, t_0^{(e)} \sim \text{Cat}(p_t)$;
 Reset $s^{(e)}$ to ref. pose $t_0^{(e)} + \text{perturbs}$;
 // Policy Optimization
 Estimate GAE \hat{A} using $\{s, a, r\}_{1:K}^{(1:N_{env})}$;
 $\theta, \phi \leftarrow \arg \max_{\theta, \phi} \mathbb{E}[\mathcal{L}_{clip} - c_v \mathcal{L}_{VF}]$;
 return θ, ϕ ;

Table 4: Reward terms for motion tracking.

Term	Formulation	Weight
Joint Position	$\exp(-\ p_j\ ^2/0.1)$	1.00
Joint Velocity	$\exp(-\ v_j\ ^2/5)$	0.50
Body Linear Velocity	$\exp(-\ v_b\ ^2/0.5^2)$	0.50
Body Angular Velocity	$\exp(-\ \omega_b\ ^2/0.5)$	0.50
Relative Body Position	$\exp(-\ p_{rel}\ ^2/0.1^2)$	1.00
Action Rate	$\ a_t - a_{t-1}\ ^2$	-0.01
Undesired Contacts	$\sum \mathbb{I}(F_c > 1.0)$	-1.00

Table 5: Domain Randomization parameters.

Category	Parameter	Type	Range
Env.	Static Friction	Uniform	[0.6, 1.0]
	Dynamic Friction	Uniform	[0.4, 0.8]
Delays	Action Delay	Uniform	[0.0, 0.02] s
Motor	Kp/Kd Factor	Scaling	[0.8, 1.2]
	Joint Armature	Scaling	[0.8, 1.2]
Body	Link Mass	Scaling	[0.8, 1.2]
	Base Mass	Additive	[-5.0, 5.0]
	Base CoM	Additive	[-0.05, 0.05] m